Observation impact over the southern polar area during the Concordiasi field campaign

Nathalie Boullot, Florence Rabier, Rolf Langland, Ron Gelaro, Carla Cardinali, Vincent Guidard, Peter Bauer, Alexis Doerenbecher

RMetS
Royal Meteorological Society

Observation impact over the southern polar area during the Concordiasi field campaign

Nathalie Boullot,[a]* Florence Rabier,[a,b] Rolf Langland,[c] Ron Gelaro,[d] Carla Cardinali,[b] Vincent Guidard,[a] Peter Bauer[b] and Alexis Doerenbecher[a]

[a]*Météo-France, National Centre for Meteorological Research (CNRM-GAME-CNRS), Toulouse, France*
[b]*European Centre for Medium-Range Weather Forecasts, Reading, UK*
[c]*Naval Research Laboratory, Monterey, CA, USA*
[d]*Global Modeling and Assimilation Office, NASA Goddard Space Flight Center, Greenbelt, MD, USA*

*Correspondence to: N. Boullot, Météo-France, CNRM/GMAP, 42 avenue Coriolis, 31057 Toulouse Cedex 1, France.
E-mail: nathalie.boullot@meteo.fr

The impact of observations on analysis uncertainty and forecast performance was investigated for austral spring 2010 over the southern polar area for four different systems (NRL, GMAO, ECMWF and Météo-France) at the time of the Concordiasi field experiment. The largest multi-model variance in 500 hPa height analyses is found in the southern sub-Antarctic oceanic region, where there are rapidly evolving weather systems, rapid forecast-error growth, and fewer upper-air wind observation data to constrain the analyses. The total impact of all observations on the model forecast was computed using the 24 h forecast sensitivity-to-observations diagnostic. Observation types that contribute most to the reduction of the forecast error are shown to be AMSU, IASI, AIRS, GPS-RO, radiosonde, surface and atmospheric motion vector observations. For sounding data, radiosondes and dropsondes, one can note a large impact on the analysis and forecasts of temperature at low levels and a large impact of wind at high levels. Observing system experiments using the Concordiasi dropsondes show a large impact of the observations over the Antarctic plateau extending to lower latitudes with the forecast range, with the largest impact around 50–70°S. These experiments indicate there is a potential benefit from using radiance data better over land and sea-ice and from innovative atmospheric motion vectors obtained from a combination of various satellites to fill the current data gaps and improve numerical weather prediction analyses in this region.

Key Words: dropsondes; forecast sensitivity to observations; observing-system experiment; forecast score

Received 6 January 2014; Revised 19 September 2014; Accepted 20 September 2014; Published online in Wiley Online Library 3 December 2014

1. Introduction

Because of the remoteness and harsh environment of the polar regions, and of the southern polar region especially, *in situ* atmospheric observations in these regions are relatively sparse. The southern polar area is particularly poorly documented by all types of observations for several reasons: it is mainly a continent over which the use of satellite radiance observations is particularly difficult because of high terrain and snow-cover, surrounded by relatively poorly observed oceans. As a result, compared with other regions of the globe, our knowledge of the atmospheric state is particularly limited. The Concordiasi project was an international collaboration which gathered innovative observations over Antarctica (Rabier *et al.*, 2010). It was a contribution to the THORPEX-IPY projects (The Observing System Research and Predictability Experiment International Polar Year projects), with the main meteorological objective to improve numerical weather prediction systems (Rabier *et al.*, 2012). The additional *in situ* observations provided by Concordiasi constitute a reference dataset which was used to compare *in situ* data with satellite retrievals (Wang *et al.*, 2013) and numerical forecasts (Cohn *et al.*, 2013) in order to document shortcomings in models and data assimilation. This knowledge can then be used to improve forecasting and assimilation and lead to more accurate real-time analyses as well as improved re-analyses.

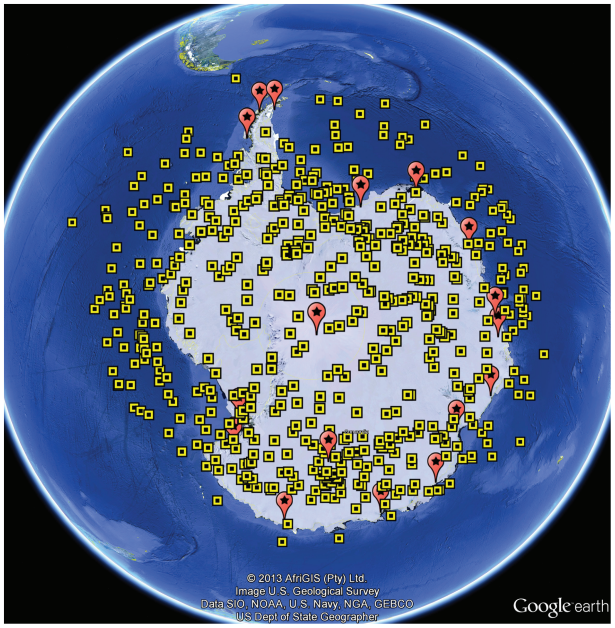

Figure 1. Map of dropsondes released over Antarctica during the Concordiasi experiment (squares). Routine radiosonde observations are shown with dots.

The additional observations were mainly intended to complement routine observations, and to match with satellite overpasses. *In situ* atmospheric observations (surface observations and upper-air profiles) are made routinely in Antarctica, but mainly along the coast (15 sites out of 17), except for the Amundsen–Scott station at the South Pole (managed by the USA) and Concordia on the plateau at Dome C (managed by Italy and France), as shown by the red dots in Figure 1. Amundsen–Scott performs two radiosoundings per day, and Concordia provides a radiosounding at 1200 UTC on most days. Concordia has the advantage of being under the swath of sun-synchronous satellites several times a day. In 2008 and 2009, the campaign was based on radiosounding measurements made primarily at Concordia to study the meteorology of the plateau in Antarctica and to provide a baseline for comparison with satellite data. In 2010, the Concordiasi project used a constellation of stratospheric long-duration instrumented balloons. The French Centre National d'Etudes Spatiales (CNES) launched 19 stratospheric balloons from the station of McMurdo in September and October 2010. Among the 19 balloons launched, 13 of them were of the 'driftsonde' type and released more than 600 dropsondes, on demand, to provide high-resolution vertical profiles of temperature, humidity, winds and pressure (Figure 1). The driftsondes (balloons and release systems of dropsondes) were developed through a partnership between CNES (responsible for the balloons) and the US National Center for Atmospheric Research (NCAR, responsible for the dropsondes and the drifting balloons: Cohn *et al.*, 2013). The drifting balloons followed the air currents in a quasi-Lagrangian way over the Antarctic for several months, at an altitude of 18 km. The release of dropsondes was mainly targeted to coincide with satellite overpasses, while some dropsondes were devoted to predictability studies and others were used to validate Global Positioning System radio-occultations (GPS-RO) measured from receivers on board the balloons (Haase *et al.*, 2012). Eventually, the dropsonde coverage was quite uniform over the southern polar area, as seen in Figure 1.

The goal of our study is to investigate the impact of polar observations (observations at latitudes poleward of 60°S) on the forecast quality over the southern polar area, with a focus on the assimilation of the additional dropsondes launched during the 2010 Concordiasi campaign. We focus on a period of interest during the 2010 campaign from 27 September to 16 November when most dropsondes were launched. Both the calculation of the impact of observations using the adjoint of a data assimilation system (e.g. Langland and Baker, 2004), but also more classical Observing-System Experiments (OSE) in the context of four-dimensional variation (4D-Var: e.g. Rawlins *et al.*, 2007) are performed. Data impacts are investigated in the numerical weather prediction systems run by four centres involved in the Concordiasi project: Météo-France (France), the Global Modeling and Assimilation Office (GMAO, USA), the Naval Research Laboratory (NRL, USA) and the European Centre for Medium-range Weather Forecasts (ECMWF). Section 2 illustrates data coverage and analysis differences in the Antarctic area. The data impact is shown with adjoint sensitivity tools in section 3 and with observing system experiments in section 4. Section 5 provides the conclusions of this study.

2. Observation coverage and analysis uncertainty in the southern polar area

In order to understand the characteristics of data assimilation systems in the southern polar area, it is relevant to investigate what is the data availability and usage. In Figure 2, the number of observations is displayed for most observation types in the NRL system. One can notice on Figure 2(a,b) the sparseness of *in situ* observations, in particular inside the Antarctic continent. One can also notice a gap in satellite-wind observation coverage. These observations, also called AMVs for Atmospheric Motion Vectors or satwind, are produced using satellite images by tracking the clouds' movements. Here, the gap can be seen by comparing Figure 2(c,d), in a zone extending from about 50 to 70°S, with geostationary winds equatorward of 50°S, and Moderate-resolution Imaging Spectroradiometer (MODIS) and Advanced Very High Resolution Radiometer (AVHRR) winds over the Antarctic continent. This is also an area where the satellite radiance usage is generally poor due to the difficulty in using radiances over sea-ice, as can be seen in Figure 2(f). However, some developments have recently taken place in Météo-France to better characterize the microwave sea-ice emissivity in order to be able to assimilate Advanced Microwave Sounding Unit B/Microwave Humidity Sounder (AMSU-B/MHS) data on this surface (Karbou *et al.*, 2013), and the coverage is then improved for this particular centre, as we can see by comparing coverage of AMSU-B/MHS between NRL in Figure 2(f) and Météo-France in Figure 3.

The assimilation of all these observations produces analysis increments, which represent the work performed by the analysis to correct the *a priori* state of the model and fit the observations. This highlights the region where uncertainties in the forecast are most reduced by the available observations. Figure 4 presents the root-mean-square (RMS) magnitude of analysis increments for the geopotential height at 500 hPa, computed for two centres, ECMWF and Météo-France. It is clear that there is a relatively small influence on the analysis by observations over the Antarctic plateau. The larger analysis increments are found in the surrounding oceans. They are larger for ECMWF than Météo-France and the maximum value is not seen at the same longitude. For ECMWF, a cross-section of analysis increments is presented in Figure 5 along 110°E across the area with maximum increments. The vertical structure shows a 10° latitudinal offset of the maximum between lower to mid-troposphere and upper troposphere to lower stratosphere. The region of large increments indicates zones of large baroclinic activity over the southern oceans. Note that sea-ice extended to about 58–60°S in September 2010 near 110°E. The vertical structure reflects the slope of the polar front.

It is also relevant to examine systematic differences in the atmospheric analyses produced by different data assimilation systems. These analysis differences represent an approximation to part of the error in estimates of the true atmospheric state, and can be found to be correlated with the distribution of *in situ* and satellite observations, and with atmospheric error growth rates (Langland *et al.*, 2008).

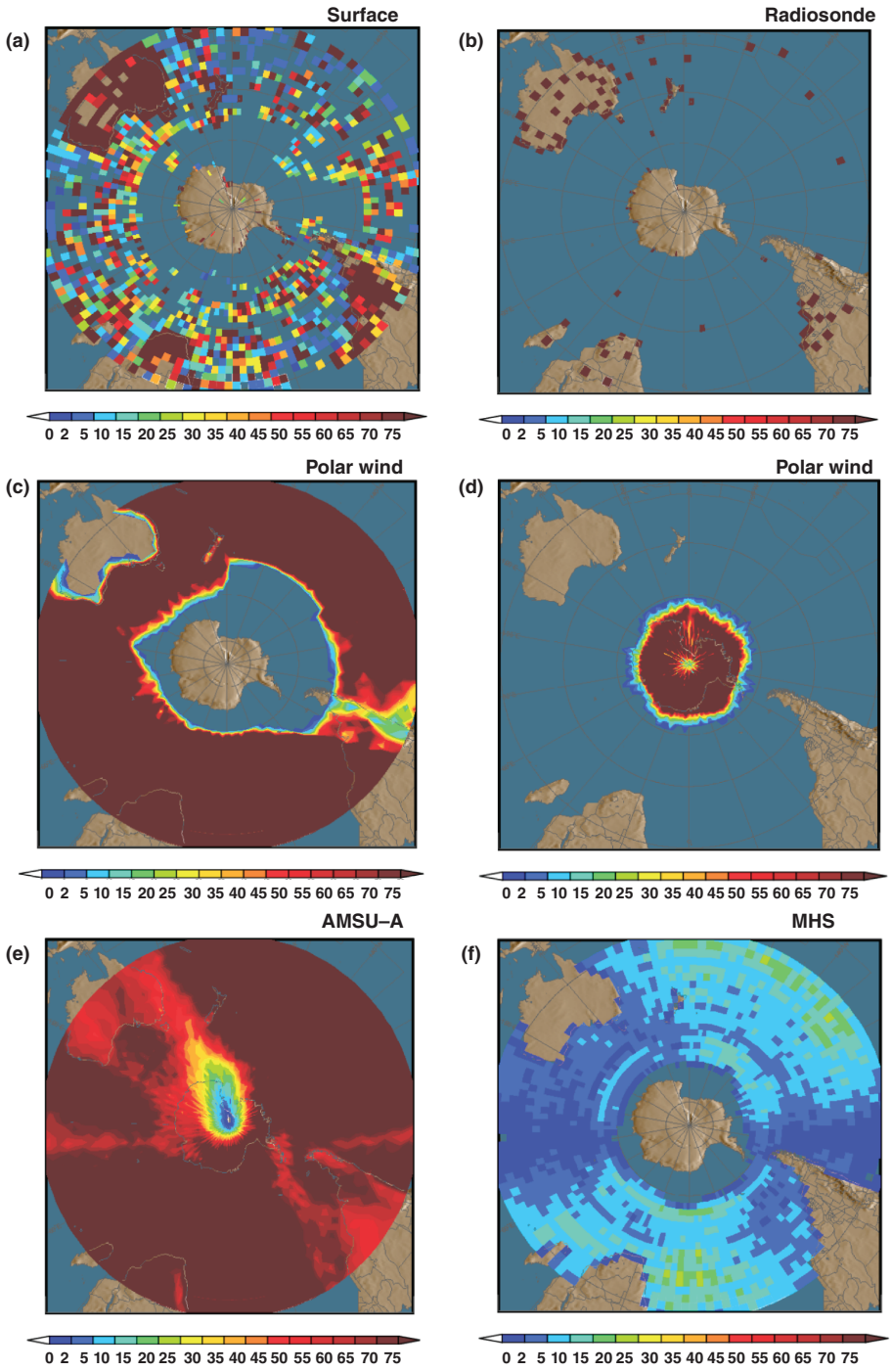

Figure 2. Maps of observations density for (a) all surface observations, (b) radiosonde, (c) satwind observations, (d) polar wind from MODIS, (e) AMSU-A, and (f) MHS observations used at NRL over 30 days (20 August to 18 September 2011).

The average 'static-time variance' of analysed 500 hPa geopotential height for 27 September to 16 November 2010 is shown in Figure 6. Here, 'static-time variance' indicates that the variance is with respect to the mean of four analyses valid at the same time. The variance is then averaged over the study period. For this quantity, large variance is found where there are frequent and relatively large differences between the four analyses. If all 500 hPa height analyses were identical at every time, the average static-time variance would be zero. Note that Figure 6 is not a variance of 500 hPa height over time.

Static-time variance in 500 hPa height analyses is due to various factors, including differences between analysis/forecast systems in observation selection, quality control, bias correction, data assimilation methodology, and in the forecast models that provide background forecasts for the data assimilation procedure. In addition, analysis differences may typically be larger in regions with strong atmospheric dynamics and rapid error growth, as found along the polar front jet, since this can create larger spread between background forecasts of the various forecast systems.

It is seen in Figure 6 that largest average static-time variance in analysed 500 hPa height for this time period is found in a zone extending from about 50 to 70°S, similar to the zonal region with large increments in Figure 4. This is a region with a relative gap in satellite-wind observation coverage, as discussed previously, and subject to strong atmospheric dynamics. The AMV gap in this region could be filled partly using AMV that combine observations from Meteorological Operational satellites METOP-A and METOP-B in the overlap region. This is under evaluation at Eumetsat. As well, the Observation-System Simulation Experiment (OSSE) study of Garand *et al.* (2013) showed that filling the AMV gap in that region from imagers on board satellites in a highly elliptical orbit would improve forecasts significantly, especially in the Southern Hemisphere. Figure 7 confirms the shape of the region with strong dynamic processes. The map shows areas of potential growth for errors in the initial

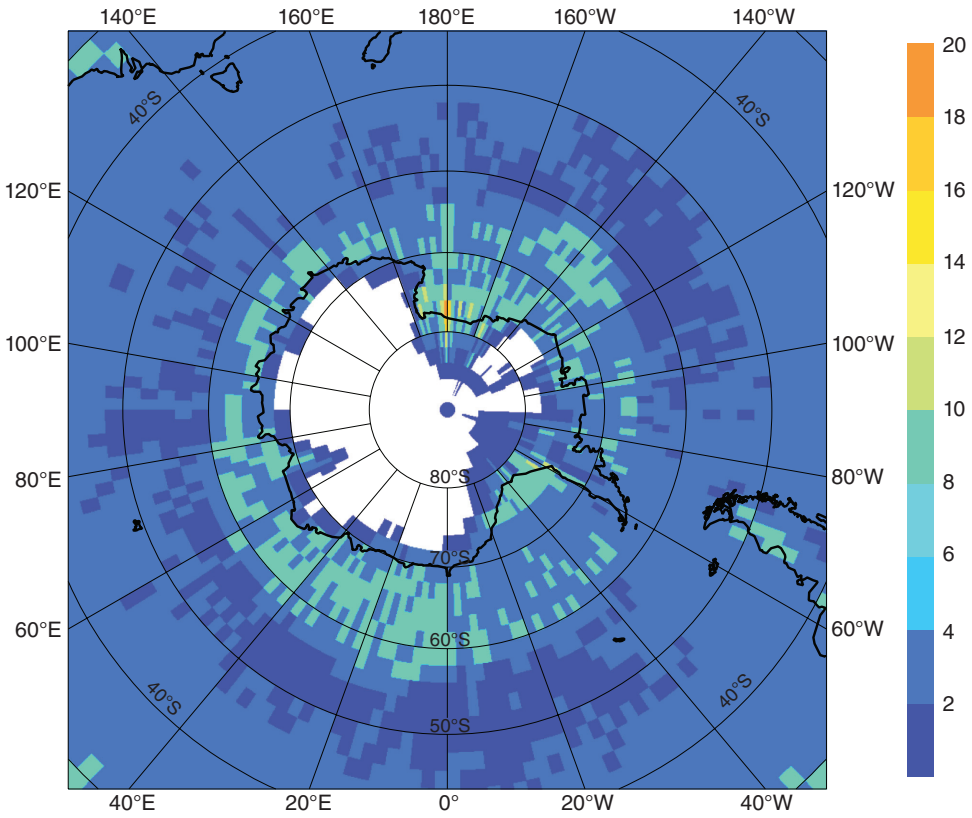

Figure 3. AMSU-B/MHS observation numbers per day in a 2° × 2° grid in the Météo-France assimilation system.

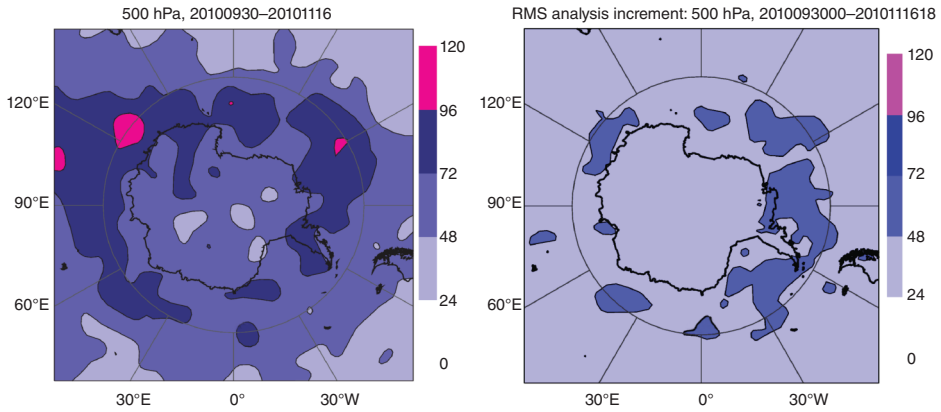

Figure 4. (a) ECMWF and (b) Météo-France root-mean-square error of analysis increments for geopotential height at 500 hPa averaged over the period ranging from end-September to mid-November 2010. Units are m.

conditions of the models. These areas are associated with the atmospheric instability. The map is the averaged singular vectors of the three-dimensional (3D) total energy vertically integrated to produce a 2D field computed over the polar region for the ECMWF system during this period. It corresponds to the areas where small perturbations of the flow will grow the fastest in the short range (Buizza and Palmer, 1995). There are three nodes along the 70°S latitude band. It is slightly more south than the signal in Figure 4, but the singular vectors were localized to account for maximal growth over the 70–90°S domain.

Static-time variance in analysed 500 hPa height is generally lower over the Antarctic continent. A major exception is observed for the region of Victoria Land, including the area around Dome C and the Concordia radiosonde station where the static-time variance is large. Apparently, during this time period, the additional Concordia radiosonde profiles were not sufficient in number to offset large variance in analysed 500 hPa height caused by factors not simply related to the number of observations. Such factors include relatively large uncertainty in background forecasts for data assimilation over this region, due to the particular difficulty in forecasting the extreme weather over the Antarctic plateau, with strong thermal inversions and strong coupling with the snow-covered surface. As explained in Cohn *et al.* (2013), all models fail to represent the strong thermal inversion with the right intensity.

Differences in static-time variance of analysed 500 hPa height from one model system to another can be quite large, as shown in Figure 8. This is an indicator of analysis reliability, since low static-time variance indicates that a particular height analysis product is consistently closer to the average of the four separate analyses. In this context, it is seen that the 500 hPa height analyses of the ECMWF (Figure 8(b)) and Météo-France (Figure 8(d)) systems have the lowest average static-time variance, while the variance of the NRL (Figure 8(c)) and GMAO (Figure 8(a)) systems are considerably larger. For each model the largest variance is found generally in the zone between 50 and 70°S, and regional maxima of variance within this latitude belt are located in the south Indian Ocean and South Pacific Ocean. Given the similarity in location of the static-time variance pattern in each model, it appears likely that this is accounted for by general properties of atmospheric dynamics and the global observing system. That is, the largest static-time variance in 500 hPa height analyses is found

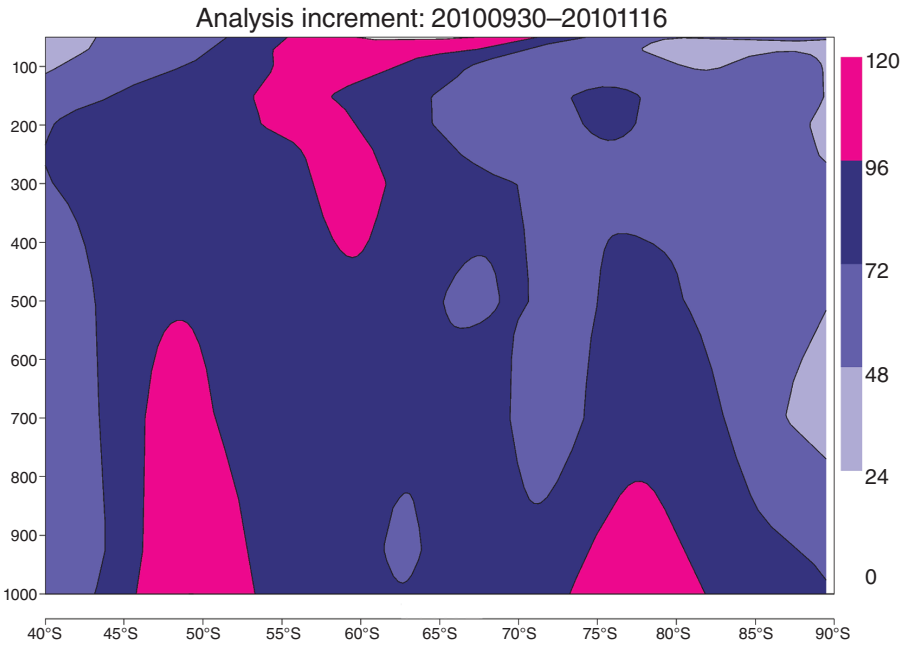

Figure 5. ECMWF cross-section along 110°E between 40 and 90°S of analysis increments root-mean-square error for geopotential height averaged over the period ranging from end-September to mid-November 2010. The vertical axis represents height in hPa and unit of the scale is m. Note that levels below ∼700 hPa south of 75°S should be discarded.

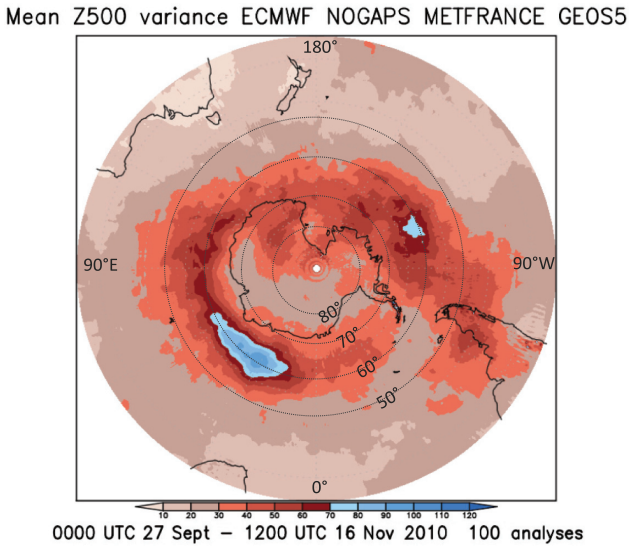

Figure 6. Average static-time variance of analysed 500 hPa geopotential height for the four models, for analyses at 0000 and 1200 UTC from 27 September to 16 November 2010. The average variance is calculated by producing an average of the four separate analyses at each analysis time (0000 and 1200 UTC daily) and taking the variance of each model's analysis from the average analysis. These variances are then summed and divided by the number of analyses, to produce the average static-time variance plot. (There are 100 separate analyses included from 27 September to 16 November 2010). Units are m^2.

in the southern sub-Antarctic oceanic region, where there are strong atmospheric dynamics, rapid forecast error growth, and fewer upper-air wind observation data to constrain the analyses. The larger static-time variance in the NRL and GMAO systems is essentially an enhancement of the variance pattern seen in the ECMWF and Météo-France analyses. NRL stands out as significantly different from the other analyses, which can be explained further from the sensitivity-to-observation experiments.

3. Data impact with the adjoint sensitivity tool

3.1. *Model descriptions and impact calculation*

The technique used to measure observation impact in this study is a variant of the method proposed by Langland and Baker (2004). It uses the adjoint of a data assimilation system to estimate the impact of individual observations on an energy-based measure of forecast error:

$$e = (\mathbf{x}^{\mathrm{f}} - \mathbf{x}^{\mathrm{t}})^{\mathrm{T}}\mathbf{P}^{\mathrm{T}}\mathbf{C}\mathbf{P}(\mathbf{x}^{\mathrm{f}} - \mathbf{x}^{\mathrm{t}}), \tag{1}$$

where $\mathbf{x}^{\mathrm{f}}$ is a 24 h forecast state, $\mathbf{x}^{\mathrm{t}}$ is the verifying analysis corresponding to $\mathbf{x}^{\mathrm{f}}$, $\mathbf{C}$ is a diagonal matrix of weights that gives units of energy per unit mass (Talagrand, 1981), $\mathbf{P}$ is a spatial projection operator that measures e only within a specified region of interest, and the superscript T denotes the transpose operation.

For the NRL, the impacts shown here are derived from the operational run of its global data Atmospheric Variational Data Assimilation System-Accelerated Representer (NAVDAS-AR: Xu *et al.*, 2005) and forecast model Navy Operational Global Atmospheric Prediction System (NOGAPS: Peng *et al.*, 2004). NAVDAS-AR uses four-dimensional variational assimilation (4D-Var) to produce analyses at 0000, 0600, 1200 and 1800 UTC, with observations assimilated during 6 h time windows using an inner-loop resolution of T119L42. The NOGAPS forecast model and its adjoint are both run at T319L42. Observation impact is measured using a moist total-energy norm evaluated over the global domain from the surface to approximately 150 hPa in the form

$$\delta e = \langle \mathbf{K}^{\mathrm{T}}\mathbf{g}, \mathbf{d}\rangle, \tag{2}$$

where $\mathbf{K}^{\mathrm{T}}$ is the adjoint of the analysis scheme, $\mathbf{d}$ are the observation-minus-background departures (innovations) and $\mathbf{g}$ is a vector in model space given by

$$\mathbf{g} = \mathbf{M}_{\mathrm{b}}^{\mathrm{T}}\mathbf{P}^{\mathrm{T}}\mathbf{C}\mathbf{P}(\mathbf{x}_{\mathrm{b}}^{\mathrm{f}} - \mathbf{x}^{\mathrm{t}}) + \mathbf{M}_{\mathrm{a}}^{\mathrm{T}}\mathbf{P}^{\mathrm{T}}\mathbf{C}\mathbf{P}(\mathbf{x}_{\mathrm{a}}^{\mathrm{f}} - \mathbf{x}^{\mathrm{t}}), \tag{3}$$

where $\mathbf{M}_{\mathrm{b}}^{\mathrm{T}}$ and $\mathbf{M}_{\mathrm{a}}^{\mathrm{T}}$ represent the adjoint of the forecast model evaluated along the forecast trajectories initialized from the background and analysis states, respectively. Equation (2) provides a nonlinear (essentially third-order) approximation of δe in terms of $\mathbf{d}$ (Errico, 2007).

Météo-France has conducted two global simulations with the 2010 version (cycle 36t1) of the French global model, Action Research Small Scale Large Scale (ARPEGE) (Fourrié *et al.*, 2006) developed in collaboration with ECMWF. It uses 4D-Var and

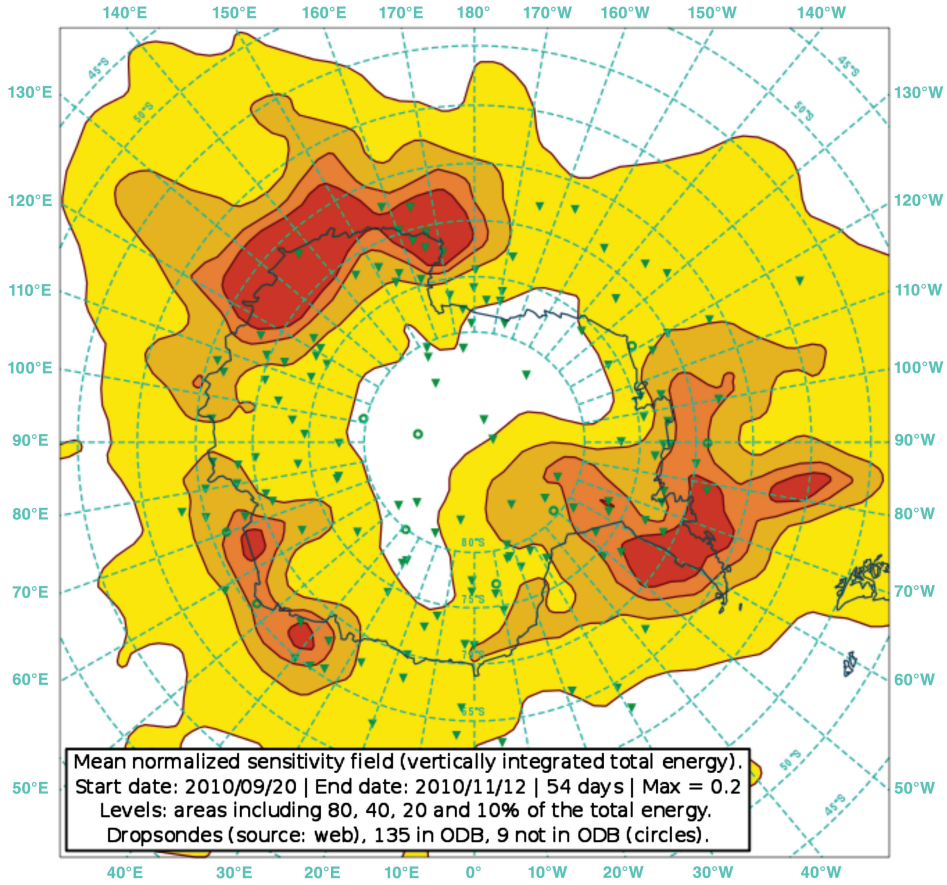

Figure 7. Averaged Singular Vectors of the 3D total energy vertically integrated to produce a 2D field for the ECMWF system (20 September–12 November 2010).

data are assimilated at 0000, 0600, 1200 and 1800 UTC with 6 h time windows. Experiments were performed for a period from 27 September to 16 November 2010, that covers the field campaign. A control experiment without the additional observations from Concordiasi was run, as well as one in which all additional observations from Concordiasi were assimilated. The stretched geometry of the model was adapted to have a better spatial resolution of about 10 km over the Antarctic and 60 km on the opposite side of the globe. Observation impacts were computed at T107 resolution based on a dry energy norm from the surface to the top of the model using Eq. (2), with $\mathbf{g}$ replaced by

$$\mathbf{g}' = \mathbf{M}_a^{\mathrm{T}}\mathbf{P}^{\mathrm{T}}\mathbf{C}\mathbf{P}(\mathbf{x}_b^f - \mathbf{x}^t) + \mathbf{M}_b^{\mathrm{T}}\mathbf{P}^{\mathrm{T}}\mathbf{C}\mathbf{P}(\mathbf{x}_a^f - \mathbf{x}^t). \qquad (4)$$

Note that Eq. (4) is similar to Eq. (3) except that the adjoint of the forecast model linearized about the forecast started from $\mathbf{x}_a$ is applied to the error measure evaluated for the forecast started from $\mathbf{x}_b$, and vice versa. This corresponds to a second-order approximation of δe in terms of $\mathbf{d}$ (Errico, 2007), but for the measure Eq. (1) provides essentially the same accuracy as the third-order form Eq. (3) (Gelaro *et al.*, 2007).

The GMAO produced a global simulation and observation impacts including Concordiasi dropsonde observations using a reduced-resolution version of the Goddard Earth Observing System 5 (GEOS-5) atmospheric data assimilation system (Rienecker *et al.*, 2007). The background forecasts and analysis increments were produced at 0.5° resolution with 72 vertical levels using the GEOS-5 forecast model and Gridpoint Statistical Interpolation (GSI: Wu *et al.*, 2002) analysis scheme, respectively. The GSI adjoint was run at 0.5° resolution, while the GEOS-5 adjoint model was run at 1° resolution. The GSI was run in a 3D-Var configuration with a 6 h update cycle. Observation impacts were computed at 0000 and 1200 UTC (although Concordiasi observations were assimilated in all cycles) based on a dry energy norm defined poleward of 60°S and from the surface to 150 hPa. The impacts were computed using a variant of the third-order approximation (Eq. (2)) which takes partial account of the multiple outer loops used to produce the forward analysis in GEOS-5, as in Gelaro *et al.* (2010).

The ECMWF operational forecast sensitivity adjoint technique uses a third-order sensitivity gradient as Langland and Baker (2004) but on a 12 h assimilation period. The sensitivity gradients (Eq. (3)) are therefore valid at the starting time of the 4D-Var assimilation window (0900 and 2100 UTC). The forecast sensitivity runs the model trajectory at the T1279 resolution whilst the linear system is solved at T255 resolution.

3.2. *Impact of the choice of domain for observations and norm definition*

Depending on the model used, the calculation of the impact of observations was performed by calculating the forecast error norm e for the whole globe or by limiting the area of interest to the southern polar region, between 60 and 90° southern latitude. In this section, we investigate how the choice of the total norm affects the impact result of an observing system. For the ARPEGE model, the calculation of the impact of observations on forecast error reduction was repeated using two different norms for the cost function calculation, a polar norm on the one hand, where e is calculated between 60 and 90°S, and a global norm on the other hand, calculated for the whole globe. This additional computation was made for a shorter period going from 8 to 31 October 2010. We focused on what we call here 'polar observations', representing observations south of 60°S. The impact of these observations in the two cases, over the same short period, is shown in Figure 9(a).

Depending on the norm used, the absolute values are not the same. However, the relative influence of each observation group is similar and almost in the same order. This shows that whichever norm is used, the relative influence of each observation group is similar for polar observations, which explains why we could compare the various systems in the previous section. The differences obtained using the global norm instead of the polar

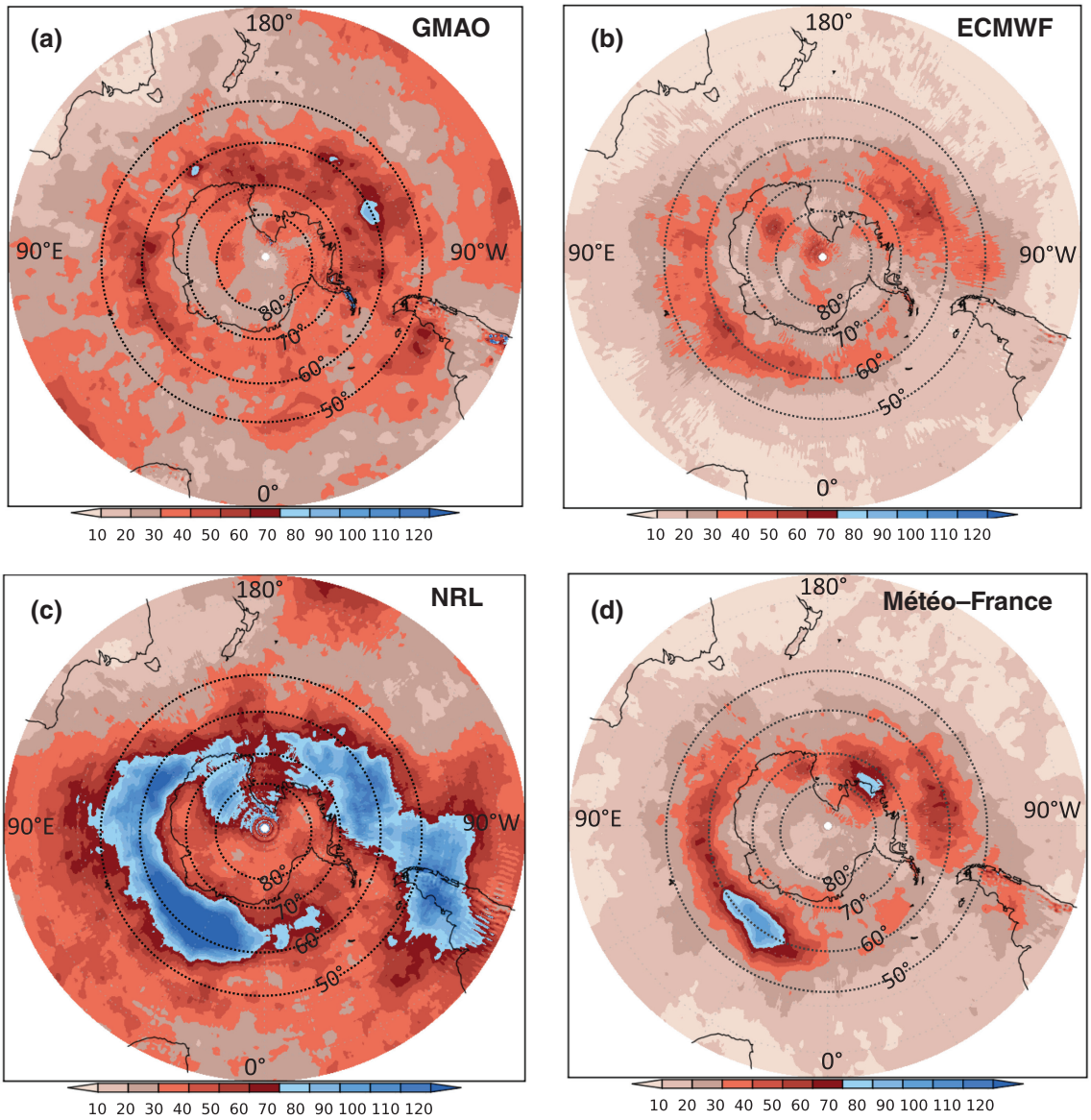

Figure 8. As in Figure 6, except showing separately the mean variance of analysed 500 hPa geopotential height in each model from the combined mean of the four fields: (a) GMAO, (b) ECWMF, (c) NRL, (d) Météo-France. Units are m^2. The time period is 0000 UTC 27 September to 1200 UTC 16 November 2010, and includes 100 analyses from each model.

norm can be interpreted as the influence of polar observations that spreads beyond their original area to the neighbouring regions in 24 h. In general, polar observations also contribute to improved forecasts.

Conversely, we can show the influence of extra polar observations on the reduction of forecast error in the polar area. Figure 9(b) shows the forecast error reduction in the Météo-France system computed only in the polar area but for all observations on one hand, and for polar observations on the other hand. Here, the relative influence of each observation group is not the same because the ocean surrounding the Antarctic area is denser in observations. Observations outside of the polar area contribute to reducing the forecast error in this area, especially AMSU-A, Infrared Atmospheric Sounding Interferometer (IASI), Synops, and buoys (exhibiting the largest differences between the two calculations in Figure 9(b)).

Although observations from outside the southern polar zone have an impact on the 24 h forecast in the polar region, polar observations are the most important, justifying our choice to focus on these particular observations.

To conclude, it is relevant to compare the impact of polar observations to the general impact of global observations. In order to compare the global observing system to what we can call the polar observing system, we show in Figure 10 the impact in the Météo-France system of different observation systems computed with different norms: global norm computed for global observations and polar norm computed only between 60 and 90° S for the polar observations.

In the global context (impact of global observation system computed with the global norm), satellite observations have the largest impact, and contribute more than 68% to the global impact. This is not surprising as they represent more than 87% of the total number of observations assimilated in this experiment. Conventional observations also play an important part and contribute to improving forecast skill. If we look more closely to the ranking, AMSU-A contribute the most, followed by IASI, radiosondes, AMVs from geostationary or polar satellites, aircraft, buoys, and radio-occultation data based on the global positioning system (GPS-RO). This is not a specific result for this assimilation and forecast system. Although the impact of any one data type depends on the mix of other data types, there is a broad consensus amongst the global numerical weather prediction (NWP) centres that these observation types are the biggest contributors to forecast skill, as noted in the final report of the fifth WMO workshop on the impact of various observing systems on numerical weather prediction (WMO, 2012).

If we focus now on the Antarctic region, we can see different features. *In situ* measurements are rare due to the hostile environment for both manual and automatic systems. In this context, satellite observations represent nearly 99% of the

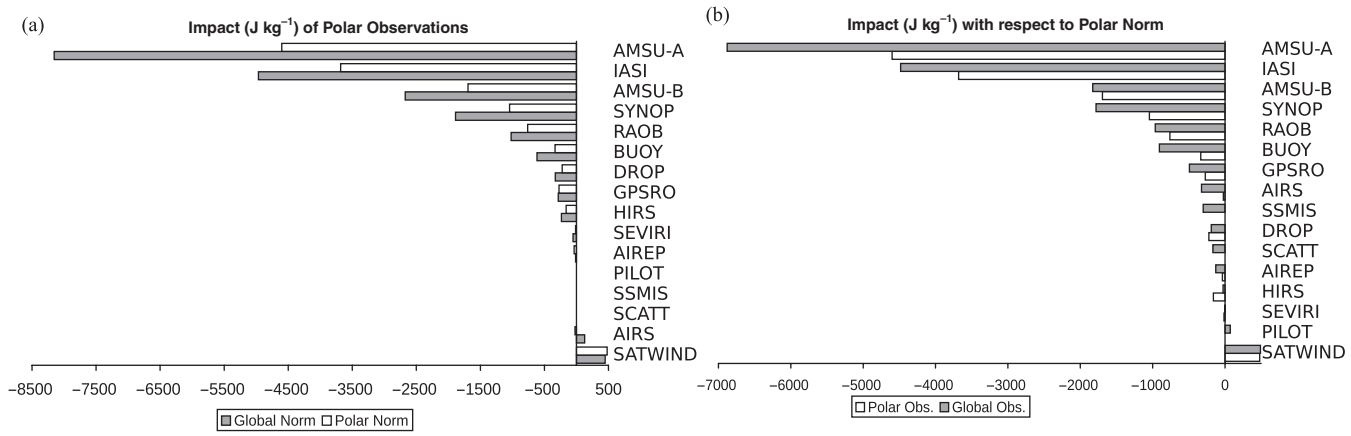

Figure 9. (a) Impact of polar observations (60–90°S) separated by observation groups when the forecast error norm e is computed for the globe (global norm, grey) or for the polar area (polar norm, white). (b) Impact of polar observations (white) and global observations (grey) using the polar norm (e computed over the polar area 60–90°S only). Both are valid for the Météo-France system, 8–31 October 2010, in J kg^{-1}.

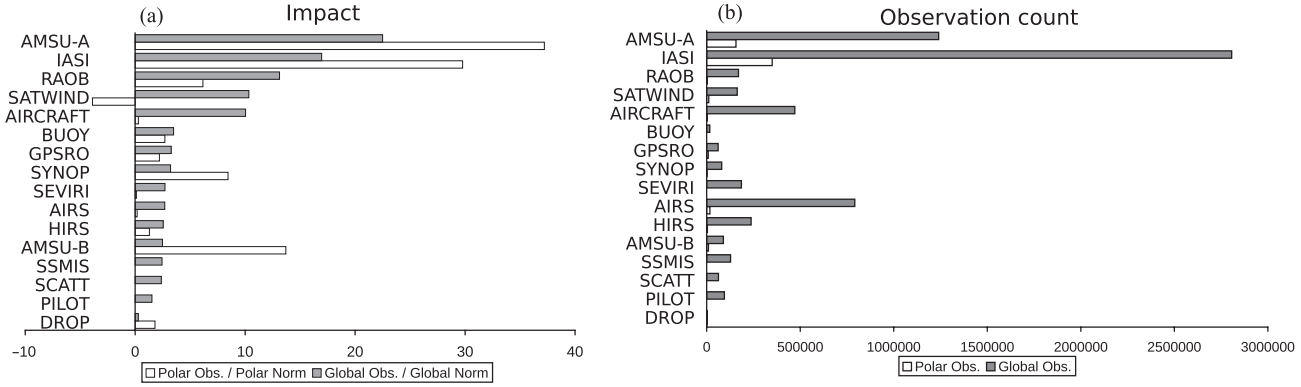

Figure 10. (a) Impact of different observation groups in Météo-France system for the polar observations using the polar norm (in white) and global observations using the global norm (in grey) computed in percentage, and (b) observation counts per day for each case.

observations assimilated, and dominate the impact. IASI and AMSU-A still represent the most important contributors to the forecast error reduction, but here the influence of AMSU-B is relatively important. AMSU-B improves the forecast in the Météo-France system as some recent progress has been made in assimilating observations over sea-ice. As explained in Karbou *et al.* (2013), the method involves estimating emissivity from the surface-sensitive observations by inverting the radiative transfer equation and assigning the retrieved surface emissivity to other sounding channels.

Although measurement stations are not numerous and observation numbers are low (0.17 and 0.44% of the total respectively), Synop and radiosondes have a good impact. Most of these measurements are made along the coast except for Amundsen–Scott at the South Pole and Concordia on the Plateau at Dome C. Drifting buoys around Antarctica also have a good impact on improving the forecast in the area. Dropsondes improve the forecast skill. Their influence in the global context is limited to 0.3%. In the polar context, it represents nearly 2% of the total impact. The low number of observations coming from aircraft explains the small influence of these observations here. The radiances from the Spinning Enhanced Visible and InfraRed Imager (SEVIRI) instrument on board the geostationary satellite Meteosat Second Generation (MSG) have little influence in polar regions as they are not numerous south of 60°S. There are no PILOT, scatterometer or Special Sensor Microwave Imager/Sounder (SSMI/S) observations assimilated in the Météo-France system in the region, mainly covered by land, sea-ice or snow and not much open sea. Surprisingly AMVs, which are one of the biggest contributors in the global context, degrade (slightly) the Météo-France forecast in the polar context during this study period. Atmospheric InfraRed Sounder (AIRS) is not assimilated over sea-ice, nor over land for the moment (even though some stratospheric and upper tropospheric channels could be assimilated). Considering High-resolution Infrared Radiation Sounder (HIRS) observations over the South Pole area (land), the Météo-France system assimilates data from only a single water vapour channel if the altitude is less than 1500 m. Over sea, observations too far from the guess for one surface channel are discarded. On the contrary, Global Positioning System Radio Occultation (GPS-RO) measurements are independent of the surface type, cloud or particles in the air and so bring a contribution commensurate with their number.

Similarly, Figure 11 shows observation impact results obtained in the NRL system. Here, in a global context, AMVs have more impact than other observation types. This may be explained largely by the greater number of AMV data assimilated, compared to other systems. Another explanation may be more-optimal assimilation of AMVs using the NRL super-observation procedure. In the polar domain, AMVs wind data (MODIS) still provide the largest forecast error reduction, followed by satellite radiances, including AMSU-A and IASI, and *in situ* measurements such as radiosondes, land-surface observations and dropsonde profiles.

3.3. Influence of polar observations in different analysis and forecast systems

We now focus on the observation impact over the southern polar area in the four different centres involved in this study. Figure 12 represents the percentage in terms of reduction of forecast error (total energy) of polar observations, namely observations polewards of 60° latitude. The total, which is different for each centre as the computation of the sensitivity of forecast error to observation is not the same, has been normalized independently for each centre so the sum of the impact is 100%. This measure does not account for the number of observations except through the impact they represent, as the relative impact of various observation types is significantly influenced by the volume of each data type.

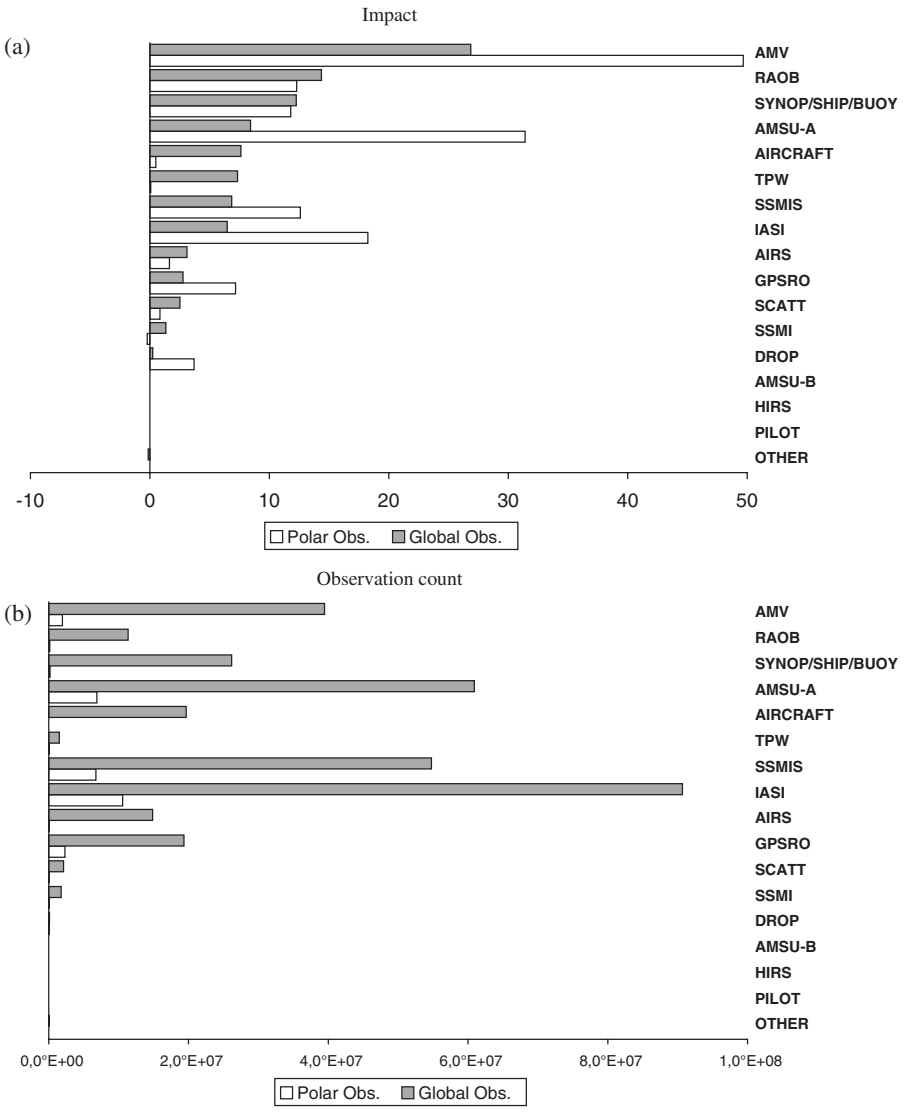

Figure 11. (a) Impact of different observation groups in NRL system for the polar observations using the polar norm (in white) and global observations using the global norm (in grey) computed in percentage, and (b) observation counts per day for each case.

The impact of the different observation groups is not distributed similarly for every system. The results obtained for each system reflect different assimilation strategies. For GMAO, Météo-France and ECMWF, 75–79% of the total forecast error reduction comes from three instruments, which are not the same for each system. For the NRL system, there are more observation sources, leaving a more evenly-spaced distribution among six of the sources. AMVs in the NRL system have the largest impact on forecast error reduction in the south polar region due to the assimilation of a larger number of MODIS and AVHRR wind data in this particular system and an elaborate pre-processing and data selection. The NRL system uses nearly 39 000 AMV observations per day, which is a little more than in the GMAO system but four times more than in the Météo-France or ECMWF system. This case notwithstanding, microwave radiances of AMSU-A and infrared radiances of IASI have a good impact in all systems, representing around 60% of the total contribution (except for NRL, for which it is 33%). The number of AMSU-A data used is similar for each centre, about 150 000 observations per day, except at ECMWF which uses nearly twice more, 313 000 observations per day in the domain of study considered, at latitudes poleward of 60°S. Compared to Météo-France for example, the ECMWF system uses one more channel and the time slots that make up the assimilation window are shorter, allowing more observations to enter the assimilation system. IASI data represent the larger volume of data assimilated for each centre, but with numbers of observations that can vary from single to double, about 500 000 observations per day for ECMWF, 350 000 observations per day for Météo-France, and 210 000 observations per day for NRL and GMAO. Indeed, the number of channels used is not the same and strategies over land and sea, and also radiance thinning or cloud detection, differ depending on the centre considered. By comparison, AIRS volume of observations is close to IASI for ECMWF, that is 400 000 observations per day, whereas the other centres only use a very small number of observations.

Météo-France shows detrimental impact of AMVs in this region, which should be investigated further (it is not generally the case, for other areas and/or other periods). AMSU-B microwave radiances account for more than 13% of total forecast error reduction in the Météo-France system only. Efforts have been made in recent years to assimilate more AMSU-A and AMSU-B radiances, particularly over land and sea-ice as discussed earlier. This is why AMSU-B impact is very important in this particular case of polar observations.

For ECMWF and Météo-France, *in situ* observations coming from Synop stations, ships and buoys play an important part in improving forecasts, representing 4.8 and 12.2% of the error reduction respectively. This is also true in the NRL system where this group of observations explains nearly 8% of the forecast error reduction. Measurements made by radiosondes contribute between 6 and 10% to the total in all systems except in the ECMWF system where they surprisingly contribute only 1.3%. In contrast, AIRS infrared data play an important part in the ECMWF system as they contribute more than 22% of the total. This is the only system where they have such a large impact.

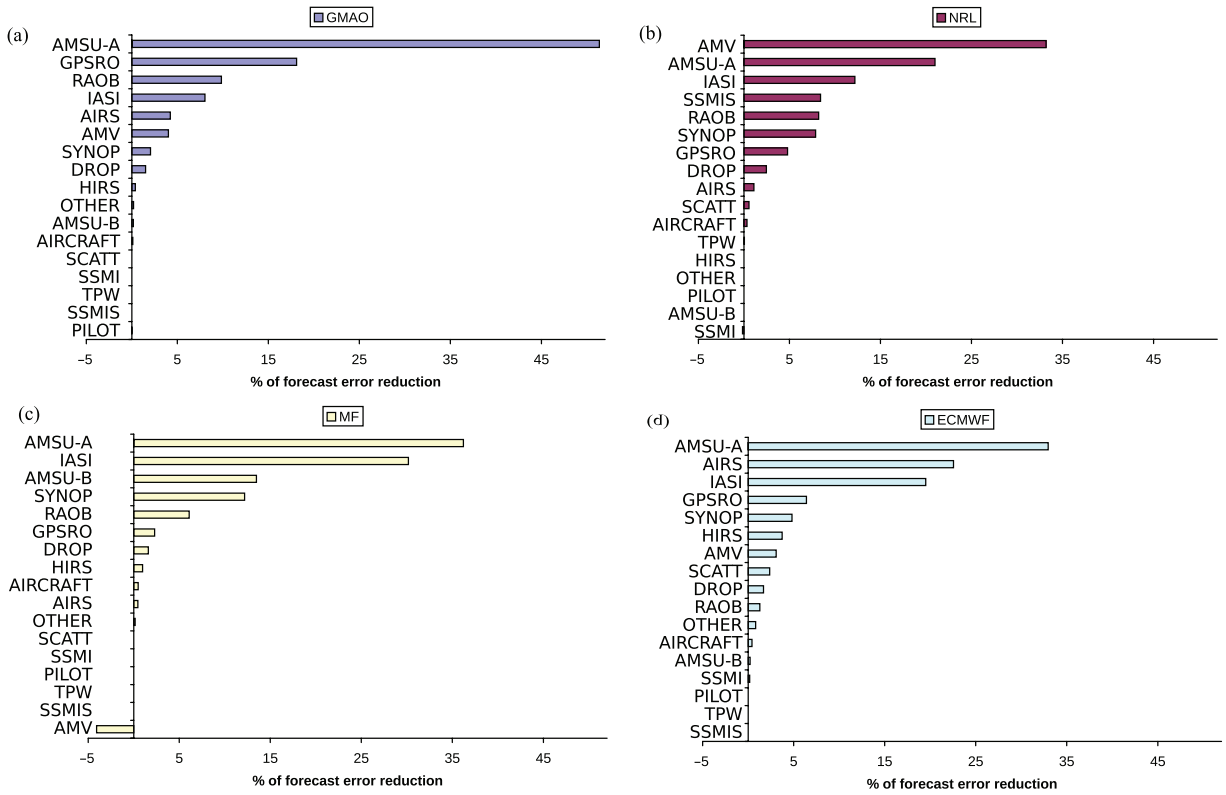

Figure 12. Normalised impact on the 24-h forecast of different observation groups in the polar domain for (a) GMAO, (b) NRL, (c) Météo-France and (d) ECMWF systems in decreasing order. The SYNOP group also includes observations from ships and buoys.

GPS radio-occultation measurements play a very important role in the GMAO system. Additionally, they contribute nearly 18% of the total impact. Although this value is less important in NRL (4.7%) and ECMWF (6.4%), this type of observation has a good impact. Météo-France is the only system less responsive to these observations with only 2.3% of the total impact. The explanation may lie in the number of observations assimilated, as they were vertically thinned in the Météo-France system to keep only one datum per model vertical layer. ECMWF and NRL use about 46 000 observations per day, 26 000 for GMAO, and only 8000 for Météo-France. This vertical thinning is not applied in the other systems. Since then, some experiments have taken place to test the assimilation of GPS-RO without any vertical thinning and up to 46 km instead of 36 km. This processing, which allows the assimilation of five times more observations and increases their impact, was subsequently implemented in operations. SSMI/S data have a relatively good impact in the NRL system (8.4%), the only system that assimilated them in this experiment.

3.4. *Dropsonde impact in the southern polar region*

During the 2010 campaign, an important effort was made to evaluate the impact of dropsonde observations. In this section, we detail the forecast improvements that dropsondes brought as part of the observing system. The impact of temperature, humidity and wind measurements are investigated as well as the impact of the location of these data.

Although the dropsonde impact is relatively small compared to satellite data such as AMSU-A, IASI or GPS-RO, it is interesting to evaluate the impact of this relatively uniform source of atmospheric profiles in the region and to compare it with the impact provided by radiosondes over Antarctica. Figure 13 shows the dropsonde impact for each measured parameter at low and high levels (below and above 400 hPa). For dropsondes at high levels, wind measurements have the largest impact, whereas temperature measurements have a large impact at lower levels. The number of observations is quite the same for wind, humidity and temperature measurements at low levels. Only humidity measurements are much less numerous in the higher layers of the atmosphere. This is particularly evident in the Météo-France system, where the influence of temperature measurements collected from dropsondes at low levels is nearly four times bigger than the influence of the wind measurements. The impact of temperature observations at high levels in GMAO and NRL systems is quite small compared to that provided by wind observations. Humidity measurements have globally a smaller impact, and a detrimental impact is seen at low levels for dropsonde humidity in the Météo-France model and for radiosonde humidity in the ECMWF model. However, one must note that humidity measurement is challenging due to the sensors' limitations. The Vaisala RS92 sensor used in the dropsondes and a large number of the radiosondes is known to have errors and biases that can vary a lot with altitude (Vömel *et al.*, 2007; Wang *et al.*, 2013). It is likely that during the assimilation process, quality controls discarded a lot of these measurements in higher layers, where errors and biases can be large.

Technically, radiosondes and dropsondes are similar as they vertically sample the atmosphere, from the bottom up for radiosondes and conversely for dropsondes. Radiosoundings are made routinely at fixed stations whereas dropsondes are launched on demand, meaning that their location and launch time are not fixed. One must note that during the assimilation process, all centres except GMAO did not consider the 4D positions and times of both radiosondes and dropsondes, meaning that the drifts of the sondes were not considered. For these two profiling methods, we can see similar features for each centre. The impact of radiosondes at low levels in the Météo-France system is more evenly distributed among temperature and wind measurements than for dropsondes. Temperature measurements at high levels in the NRL system have a bigger impact than for dropsondes.

Most radiosondes in Antarctica are launched along the coast, except for the Amundsen–Scott station at the South Pole and Concordia station at Dome C. In contrast, dropsondes were deployed in many different locations, some of them over the surrounding oceans, others over the Antarctic continent. This allowed sampling of the atmosphere at latitudes usually poorly covered by *in situ* observations.

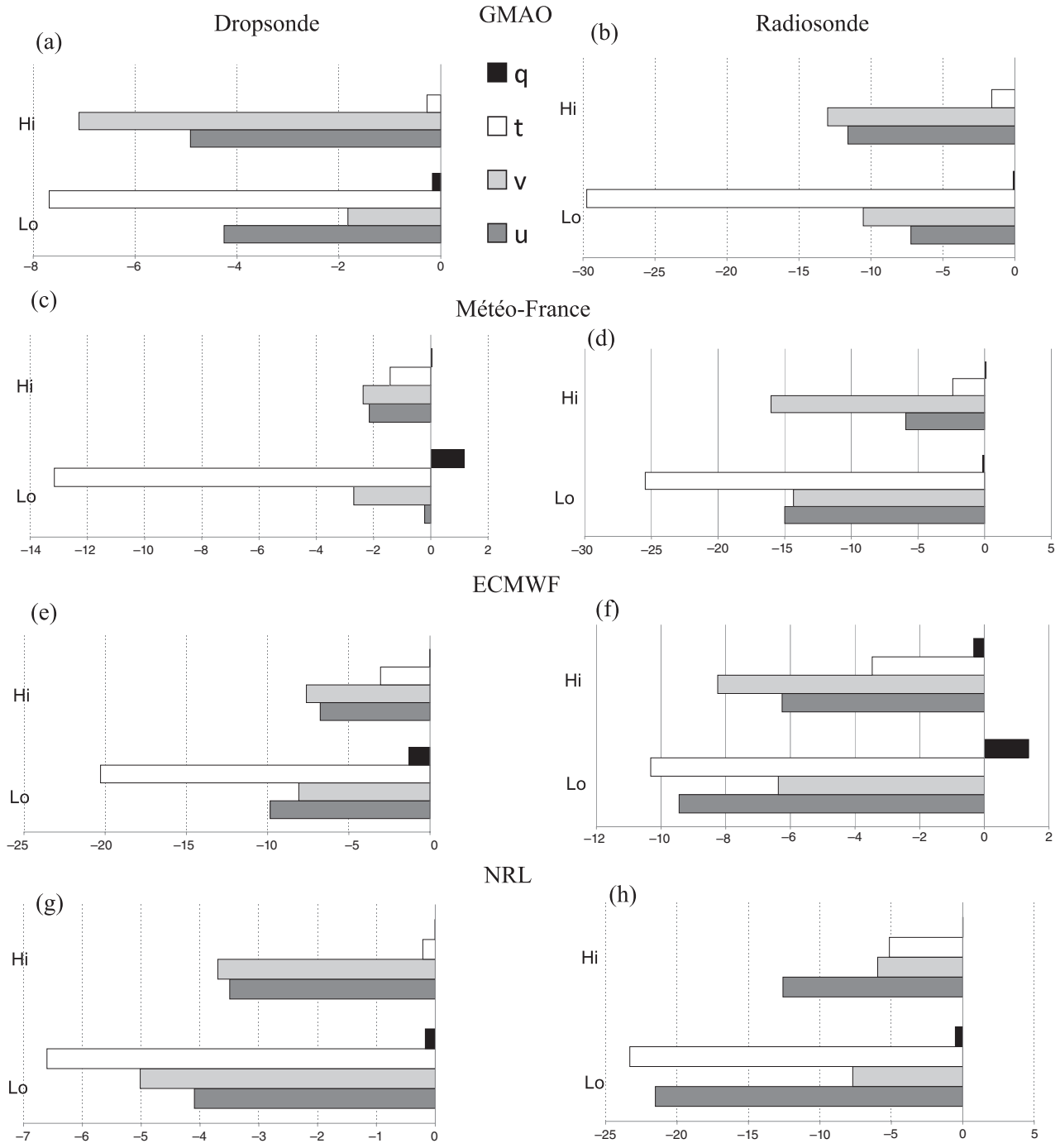

Figure 13. Impact of (a,c,e,g) dropsondes and (b,d,f,h) radiosonde data by parameter (u, v, t, q) and layer (Hi, Lo). The low layer (Lo) is for pressure greater than 400 hPa and the high layer (Hi) is for pressure less than 400 hPa in different systems: (a) and (b) GMAO, (c) and (d) Météo-France, (e) and (f) ECMWF, (g) and (h) NRL. Negative values correspond to a reduction in forecast error. Impact values on the abscissa have been normalised so that the total impact of dropsondes or radiosondes is 100% for each centre.

In order to further investigate the improvement brought by dropsondes over Antarctica, impacts of individual observations have been computed and the results gathered in three latitude bands of 10° each between 60 and 90°S. The result for each centre is shown in Figure 14.

We consider here the impact per observation for dropsondes, not the total impact. In the GMAO and Météo-France systems, individual observations have the largest impact when located near the South Pole. For the ECMWF and the NRL system, observations located on a ring between 60 and 70°S participate more in reducing the forecast error. The intermediate ring between 70 and 80°S is the location where observations have the smallest impact per observation. These differences may be explained by several considerations. Impact per observation results are basically controlled by a combination of observation density and observation sensitivity. The 80–90°S band has few regular observations and the added dropsondes have a relatively high impact per observation. The 70–80°S band includes some of the main Antarctic radiosondes and land-surface observation stations (McMurdo, Vostok, Dome C), so dropsondes here are competing with impact from existing radiosonde stations, and should have less impact per observation. There is more cyclone activity in the 60–70°S latitude band, but this band is outside the range of AMV coverage. So these challenging forecast areas may benefit from the dropsondes as additional data to improve the analysis, and the impact per observation is higher in these latitudes.

For the GMAO and Météo-France systems, the domain used to compute the impact of the observations is the southern polar area, which might explain the relatively larger values for the higher latitudes. On the contrary, the domain used to compute the impact of the observations in the ECMWF and NRL systems is global, which might explain the larger values for the lower latitude bands for these two systems.

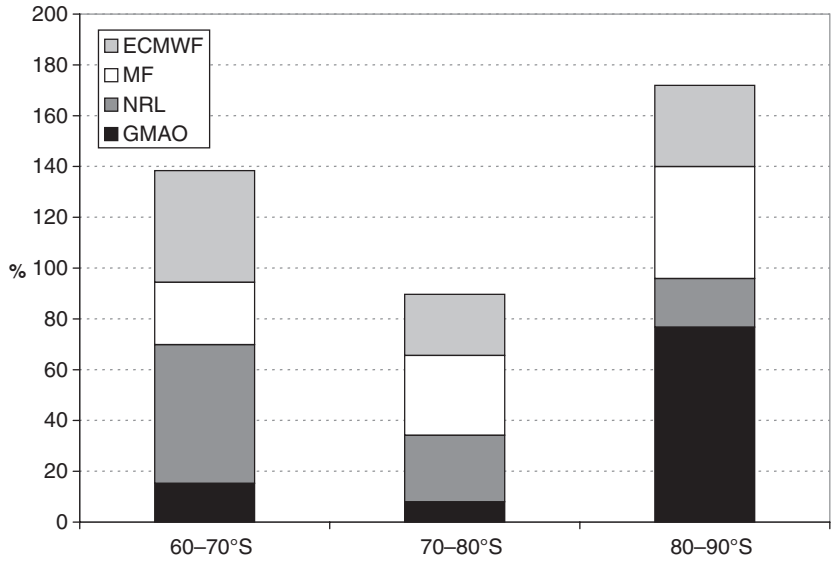

Figure 14. Impact per observation of dropsonde data in different systems by latitude bands 10° wide. Impacts are normalised for each system (GMAO, NRL, Météo-France and ECMWF) for the sum of three columns to be 100% for each centre over the polar area (60–90°S).

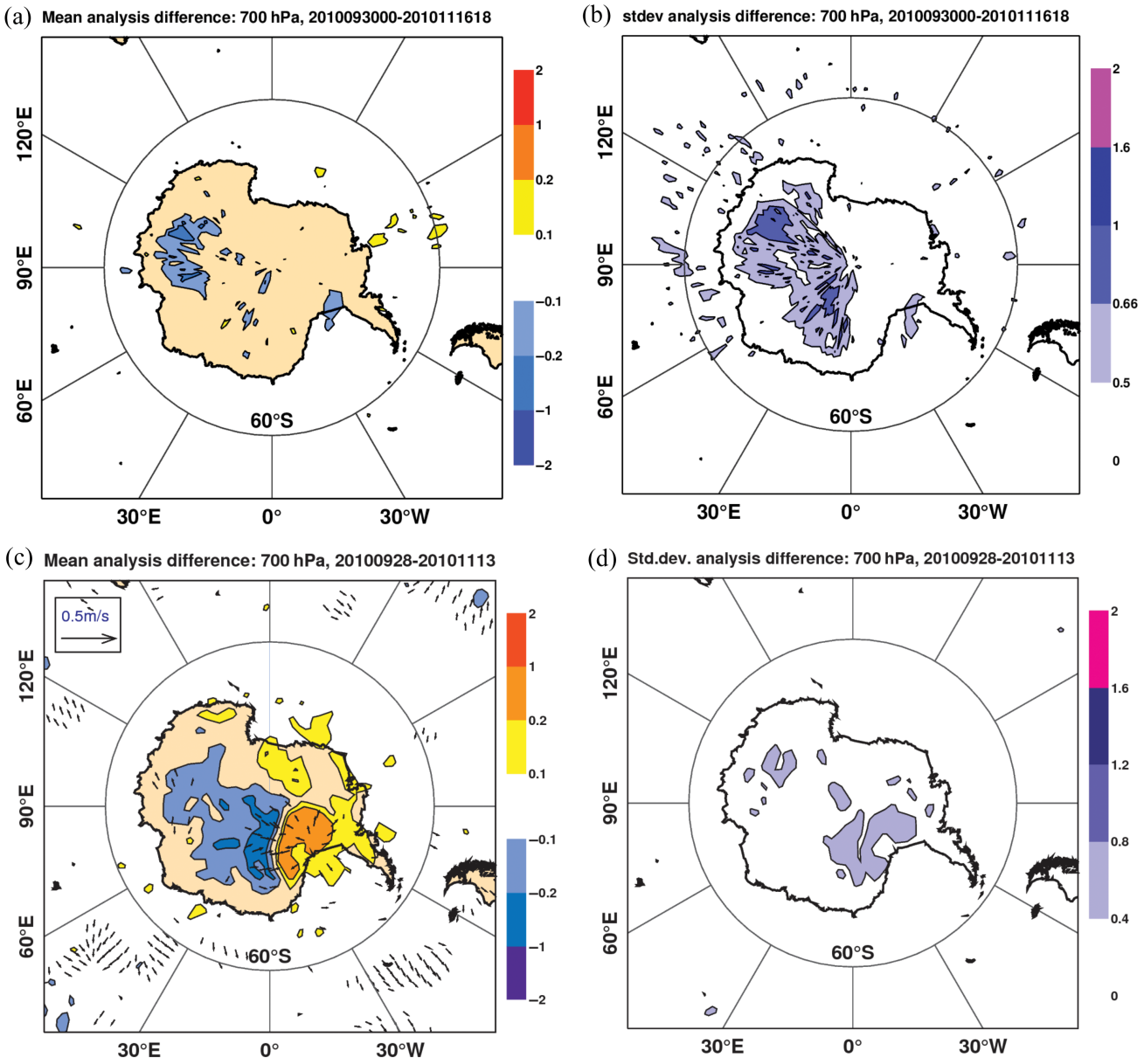

Figure 15. Temperature (control-dropsonde denial) difference fields (K) at 700 hPa for Météo-France (a) mean analysis difference, (b) standard deviation of analysis difference, and for ECMWF (c) mean analysis difference for temperature and wind and (d) standard deviation.

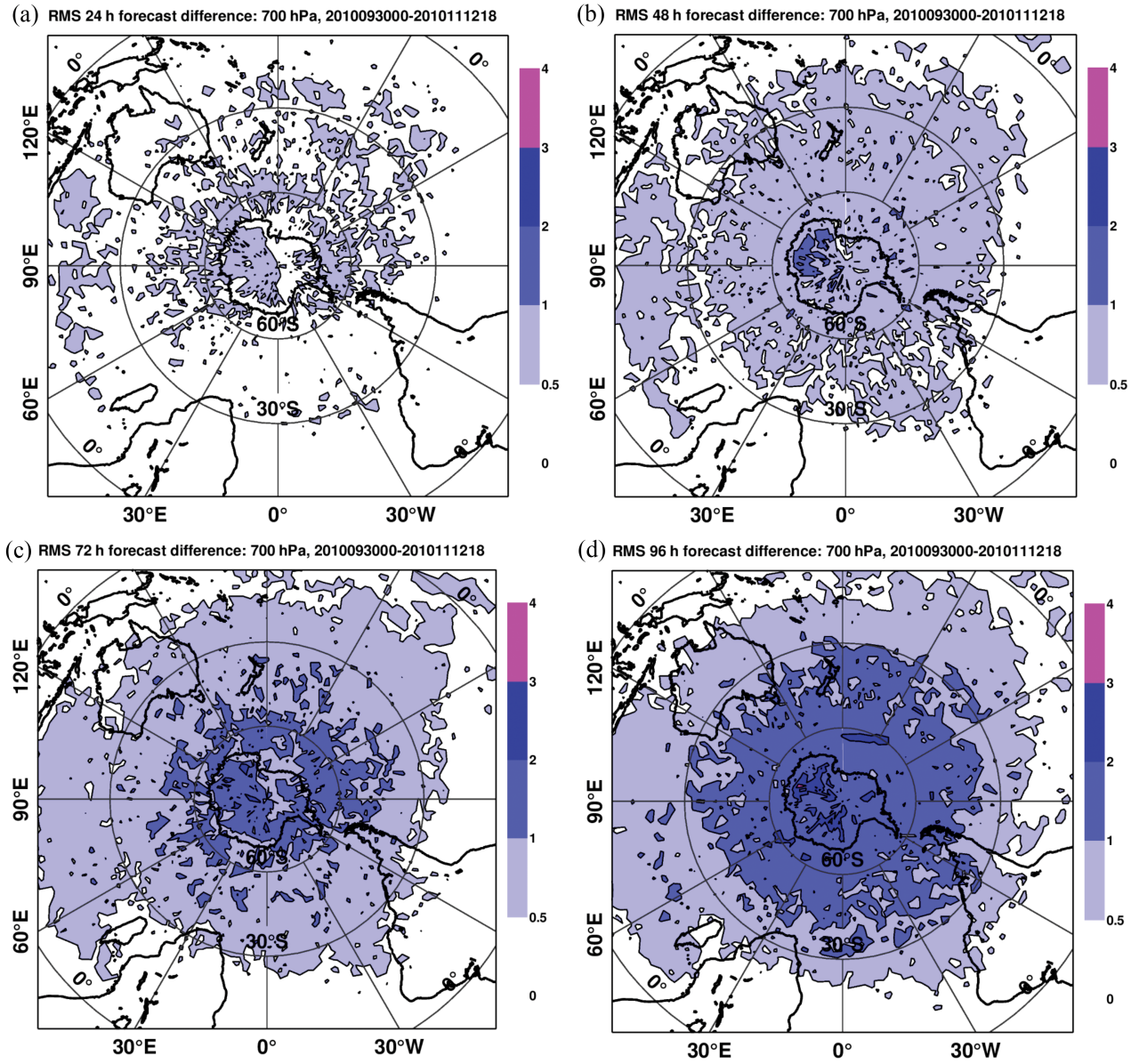

Figure 16. Météo-France temperature difference (control-denial) fields (K) at 700 hPa. (a) RMS of 24 h forecast difference, (b) RMS of 48 h forecast difference, (c) RMS of 72 h forecast difference, (d) RMS of 96 h forecast difference.

4. Observing-system experiments

ECMWF and Météo-France performed observing-system experiments to document further the impact of the Concordiasi dropsondes. Experiments with and without the dropsonde data were run from the end of September to mid-November 2010, when most of the 644 dropsondes were available. At ECMWF, the experiments were performed using the operational Integrated Forecast System (IFS) cycle 36R4 at the resolution T799 for the model trajectory (and forecast) with three inner loops at T159, T255 and T255 for the analysis resolution. The reference experiment contains all the operational data plus the dropsondes observations.

The examination of analysis differences showed that, as anticipated from the results described in the previous section, these data provide most of the impact in winds at higher altitudes and temperature at lowest altitudes. An example is shown in Figure 15, for the analysis temperature differences at 700 hPa, applied to both Météo-France and ECMWF, for both averaged differences and standard deviations of differences.

The changes to the analysis from the dropsondes are not in the areas with large uncertainty of analysed height (Figure 6) or with large singular vector amplitude (Figure 7). Also, ECMWF has larger analysis differences (Figure 15(c)), which is consistent with Figure 13. The average impact over the Antarctic plateau is to lower the temperature, which is consistent with a compensation of the model biases (Cohn *et al.*, 2013; Rabier *et al.*, 2013). The models are not cold enough over the plateau and the dropsondes manage to correct part of this bias. Inland Antarctica is also the place where the analysis differences have the largest standard deviations. This shows that at this relatively low level, the dropsondes mainly introduce differences over inland Antarctica.

One can investigate how this analysis impact translates into a forecast impact. The RMSs of the differences between the experiments with and without the dropsondes are plotted in Figure 16 for the Météo-France experiment at forecast ranges from 1 to 4 days. One can see how the initial differences grow in time to extend to lower latitudes. Although the largest forecast impact remains over inland Antarctica, it is also significant around 60°S for most of the forecast ranges.

5. Conclusions

In this article, the impact of observations on analysis uncertainty and forecast performance was investigated for austral spring 2010 over the southern polar area for four different systems (NRL, GMAO, ECMWF and Météo-France). The period of interest was chosen so as to coincide with the main field observation campaign of the Concordiasi project, providing more than 600 additional

dropsonde atmospheric profiles over the area. Examination of the observation coverage and analysis differences between the four centres point out an area of poor data density and maximum analysis uncertainty over the southern ocean at latitudes ranging from 50 to 70°S. This is also an area with large flow instability as shown by the singular vectors. The impact of observations was then calculated with the adjoint method and shows similarities between the four systems. Instruments that have the largest impact are AMSU, IASI, AIRS, GPS-RO, RAOB, surface and AMV data; however, the exact ranking varies among centres due to their data assimilation system specifications. The NRL shows a particularly strong impact of AMV data, as this centre uses more of these observations than the other centres or over-weights AMVs. Another explanation may be that radiance assimilation is not as optimum as that at other centres because of bias in the NRL forecast model. The Météo-France assimilation exhibits a large impact of AMSU-B data, following some research developments to be able to use these data over sea-ice. Compared to the global context, there is generally more impact of satellite data and less impact of conventional observations. This would be slightly different over the northern polar area, where radiosondes and aircraft play a more prominent role (not shown). For sounding data over Antarctica, one can note a large impact of temperature at low levels and a large impact of winds at high levels. In terms of impact by latitude band, both the area near to the pole and the latitudes around 60°S where dynamic instability prevails show a large impact per observation. Observing System Experiments using the Concordiasi dropsondes show a large impact of the observations over the Antarctic plateau extending to lower latitudes with the increasing forecast range, with a large impact around 60°S.

This study was primarily aimed at documenting data impact over the southern polar area to highlight the importance of certain data types and point to the use of additional observations. In particular, a better use of satellite data over snow and sea-ice would improve model temperature at low altitudes. Another promising data source is the AMVs provided by a combination of geostationary and polar-orbiting satellites, which are precisely located in the 'ring of uncertainty' between 50 and 70°S. AMVs obtained combining METOP-A and METOP-B observations in the overlap region could be of great interest to fill the gap in this region.

Acknowledgements

Concordiasi is an international project, supported by the following agencies: Météo-France, CNES, CNRS/INSU, NSF, NCAR, University of Wyoming, Purdue University, University of Colorado, the Alfred Wegener Institute, the Met Office and ECMWF. Concordiasi also benefits from logistic or financial support of the operational polar agencies IPEV, PNRA, USAP and BAS, and from BSRN measurements at Concordia. Concordiasi is part of the THORPEX-IPY cluster within the International Polar Year effort. The authors would like to acknowledge Cihan Sahin (ECMWF) for providing the singular vectors optimised over the southern polar area during the Concordiasi experiment.

References

Buizza R, Palmer TN. 1995. The singular-vector structure of the atmospheric general circulation. *J. Atmos. Sci.* **52**: 1434–1456.

Cohn SA, Hock T, Cocquerez P, Wang JH, Rabier F, Parsons D, Harr P, Wu C-C, Drobinski P, Karbou F, Venel S, Vargas A, Fourrié N, Saint-Ramond N, Guidard V, Doerenbecher A, Hsu H-H, Lin P-H, Chou M-D, Redelsperger J-L, Martin C, Fox J, Potts N, Young K, Cole H. 2013. Driftsondes: providing *in situ* long-duration dropsonde observations over remote regions. *Bull. Am. Meteorol. Soc.* **94**: 1661–1674.

Errico RM. 2007. Interpretation of an adjoint-derived observational impact measure. *Tellus* **59A**: 273–276.

Fourrié N, Marchal D, Rabier F, Chapnik B, Desroziers G. 2006. Impact study of the 2003 North Atlantic THORPEX regional campaign. *Q. J. R. Meteorol. Soc.* **132**: 275–295.

Garand L, Feng J, Heilliette S, Rochon Y, Trishchenko AP. 2013. Assimilation of circumpolar wind vectors derived from highly elliptical orbit imagery: impact assessment based on observing system simulation experiments. *J. Appl. Meteorol. Clim.* **52**: 1891–1908, doi: 10.1175/JAMC-D-12-0333.1.

Gelaro R, Zhu Y, Errico RM. 2007. Examination of various-order adjoint-based approximations of observation impact. *Meteorol. Z.* **16**: 685–692.

Gelaro R, Langland RH, Pellerin S, Todling R. 2010. The THORPEX observation impact intercomparison experiment. *Mon. Weather Rev.* **138**: 4009–4025.

Haase JS, Maldonado-Vargas J, Rabier F, Cocquerez P, Minois M, Guidard V, Wyss P, Johnson AV. 2012. A proof-of-concept balloon-borne Global Positioning System radio occultation profiling instrument for polar studies. *Geophys. Res. Lett.* **39**: L02803, doi: 10.1029/2011GL049982.

Karbou F, Rabier F, Prigent C. 2013. The assimilation of observations from the Advanced Microwave Sounding Unit over sea ice in the French global numerical weather prediction system. *Mon. Weather Rev.* **142**: 125–140.

Langland RH, Baker NL. 2004. Estimation of observation impact using the NRL atmospheric variational data assimilation adjoint system. *Tellus* **56A**: 189–201.

Langland RH, Maue RN, Bishop CH. 2008. Uncertainty in atmospheric temperature analyses. *Tellus* **60A**: 598–603.

Peng MS, Ridout JA, Hogan TF. 2004. Recent modification of the Emanuel convective scheme in the Navy Operational Global Atmospheric Prediction System. *Mon. Weather Rev.* **132**: 1254–1268.

Rabier F, Bouchard A, Brun E, Doerenbecher A, Guedj S, Guidard V, Karbou F, Peuch V-H, El Amraoui L, Puech D, Genthon C, Picard G, Town M, Hertzog A, Vial F, Cocquerez P, Cohn SA, Hock T, Cole H, Fox J, Parsons D, Powers J, Romberg K, VanAndel J, Deshler T, Mercer J, Haase JS, Avallone L, Kalnajs L, Mechoso CR, Tangborn A, Pellegrini A, Frenot Y, McNally A, Thépaut J-N, Balsamo G, Steinle P. 2010. The Concordiasi project in Antarctica. *Bull. Am. Meteorol. Soc.* **91**: 69–86, doi: 10.1175/2009BAMS2764.1.

Rabier F, Cohn S, Cocquerez P, Hertzog A, Avallone L, Deshler T, Haase J, Hock T, Doerenbecher A, Wang JH, Guidard V, Thépaut J-N, Langland R, Tangborn A, Balsamo G, Brun E, Parsons D, Bordereau J, Cardinali C, Danis F, Escarnot J-P, Fourrié N, Gelaro R, Genthon C, Ide K, Kalnajs L, Martin C, Meunier L-F, Nicot J-M, Perttula T, Potts N, Ragazzo P, Richardson D, Sosa-Sesma S, Vargas A. 2012. The Concordiasi field experiment over Antarctica: first results from innovative atmospheric measurements. *Bull. Am. Meteorol. Soc.* **94**: ES17–ES20, doi: 10.1175/BAMS-D-12-00005.1.

Rabier F, Thépaut J-N, Saint-Ramond N, Guidard V, Karbou F, Vincensini A, Langland R, Gelaro R, Cardinali C, August T, Fourrié N, Doerenbecher A, Guedj S, Bauer P, Richardson D, Janousek M, Sahin C, Garcia-Mendez A, Parrett C, Saunders R, Cress A, Pflüger U, Verner G, Koclas P, Sato Y, Ling Y. 2013. 'Model performance and data impact over polar regions'. In *Proceedings from the ECMWF/WWRP Polar Workshop*, 24–27 June 2013. Reading, UK.

Rawlins F, Ballard SP, Bovis KJ, Clayton AM, Li D, Inverarity GW, Lorenc AC, Payne TJ. 2007. The Met Office global four-dimensional variational data assimilation scheme. *Q. J. R. Meteorol. Soc.* **133**: 347–362.

Rienecker MM, Suarez MJ, Todling R, Bacmeister J, Takacs L, Liu HC, Gu W, Nielsen E. 2007. 'The GEOS-5 data assimilation system: a documentation of GEOS-5.0', NASA Technical Report 104606, Vol. 27.

Talagrand O. 1981. A study of the dynamics of four-dimensional data assimilation. *Tellus* **33**: 43–60.

Vömel H, Selkirk H, Miloshevich L, Valderde-Canossa J, Valdés J, Kyrö E, Kivi R, Stolz W, Peng G, Diaz JA. 2007. Radiation dry bias of the Vaisala RS92 humidity sensor. *J. Atmos. Oceanic Technol.* **24**: 953–963.

Wang JH, Zhang LY, Dai AG, Immler F, Sommer M, Vömel H. 2013. Radiation dry bias correction of Vaisala RS92 humidity data and its impacts on historical radiosonde data. *J. Atmos. Oceanic Technol.* **30**: 197–214.

WMO. 2012. In *Final Report of the Fifth WMO Workshop on the Impact of Various Observing Systems on Numerical Weather Prediction*, 22–25 May 2012. Technical report 2012-1, WMO Integrated Global Observing System, Sedona, AZ. http://www.wmo.int/pages/prog/www/OSY/Meetings/NWP5_Sedona2012/Final_Report.pdf (accessed 05 November 2014).

Wu W-S, Purser RJ, Parrish DF. 2002. Three-dimensional variational analysis with spatially inhomogeneous covariances. *Mon. Weather Rev.* **130**: 2905–2916.

Xu L, Rosmond T, Daley R. 2005. Development of NAVDAS-AR: formulation and tests of the linear problem. *Tellus* **57A**: 546–559.